Mater.Phys.Mech. 5 (2002) 23-30

CALORIMETRIC MEASUREMENTS OF GRAIN GROWTH IN ULTRAFINE-GRAINED NICKEL

A.P. Zhilyaev [1,3], G. V. Nurislamova [2], S. Suriñach [3], M. D. Baró [3] and T. G. Langdon [4]

[1] Institute of Mechanics, Russian Academy of Science, 450000 Ufa, Russia
[2] Institute for Physics of Advanced Materials, Ufa State Aviation Technical University, 450000 Ufa, Russia
[3] Universitat Autònoma de Barcelona, 08193 Bellaterra, Spain
[4] Departments of Aerospace & Mechanical Engineering and Materials Science, University of Southern California, Los Angeles, CA 90089-1453, USA

Received: April 06, 2002

Abstract. The process of grain growth in ultrafine-grained nickel was studied using differential scanning calorimetry. Samples of nickel, with mean grain sizes in the range from 100 to 400 nm, were prepared by equal-channel angular pressing, high pressure torsion or combinations of both. It is shown using differential scanning calorimetry that grain growth in these structures begins at temperatures in the range from 500 to 700K and the measured activation energy for grain growth is close to the activation energy for grain boundary self-diffusion. There was also evidence for a decreasing activation energy in the samples prepared by high pressure torsion.

1. INTRODUCTION

There are two important techniques for refining the microstructure of metals and alloys without contamination and without creating any internal porosity: these techniques are high-pressure torsion (HPT) and equal-channel angular pressing (ECAP) and they represent two examples of processing through severe plastic deformation (SPD) [1]. Combinations of these techniques are also effective in refining the microstructure. A series of recent reports described the microstructural evolution occurring in pure nickel after processing using HPT [2] or ECAP [2-4]. These results demonstrate that the microstructure of nickel samples can be refined to mean grain sizes of the order of ~0.35 μm by ECAP [3, 4] and ~0.17 μm by HPT [2]. It is shown in the present work that even greater grain refinement may be achieved by using a combination of ECAP and HPT.

Ultrafine-grained (UFG) and nanoscale materials generally have a low thermal stability because they are in a metastable condition. Therefore, relaxation and grain growth may occur at significantly lower temperatures than in conventional coarse-grained materials. Also, thermally activated processes (for example, grain boundary diffusion) may have lower activation energies in these materials than in similar materials with large grain sizes. For example, there is evidence suggesting that grain boundary diffusion of copper in UFG nickel differs by orders of magnitude from conventional grain boundary diffusion in coarse-grained nickel [5]. On the other hand, an evaluation of the activation energy for grain growth in ECAP nickel yielded a value close to that anticipated for self-diffusion in nickel [3] and similar results were reported also for grain growth in an electrodeposited nanocrystalline nickel [6, 7].

The present investigation was initiated to address this apparent discrepancy. Specifically, tests were undertaken to determine the activation energy and released enthalpy associated with grain growth occurring in pure nickel processed by ECAP, HPT, cold rolling (CR) and their combinations using differential scanning calorimetry (DSC).

Corresponding author: A.P. Zhilyaev, e-mail: AlexZh@mail.rb.ru

2. EXPERIMENTAL MATERIAL AND PROCEDURES

The principles of processing by ECAP and HPT have been described in several papers [1-4, 8]. Briefly, nickel cylinders having diameters of 16 mm and lengths of ~100 mm were subjected to ECAP at room temperature using a die with an internal angle of 90°. Samples were pressed repetitively for 8 passes, equivalent to a total strain of ~8, and each sample was reversed from end to end and rotated by 90° about the longitudinal axis between passes. Earlier experiments showed this procedure produces an as-pressed mean grain size of ~0.30-0.35 μm [3, 4]. For processing by HPT, disks with diameters of 10 mm and thicknesses of ~0.3 mm were torsionally strained under a high pressure of 6 GPa for a total of 5 complete revolutions, equivalent to a true logarithmic strain ~6. This procedure produces a mean grain size of ~0.17 μm [2]. Three additional samples were prepared by using an electrodischarge procedure to cut disks from the central parts of rods prepared by ECAP and then subjecting these disks to one of the following procedures. First, a disk was processed by HPT for 5 revolutions under an applied pressure of 6 GPa: this sample is designated ECAP+HPT. Second, a disk was cold rolled to give a reduction in thickness from 1.7 to 0.25 mm, equivalent to a reduction of ~85%: this sample is designated ECAP+CR. Third, a cold-rolled sample was further subjected to HPT for 5 turns under an applied pressure of 6 GPa: this sample is designated ECAP+CR+HPT. In addition, a sample of electrodeposited nanocrystalline nickel with a grain size of ~35 nm was also included for comparison. Following processing, the microstructures of these various samples were examined using transmission electron microscopy (TEM).

The thermal behavior of these samples was evaluated using DSC under an atmosphere of pure argon. All DSC measurements were performed in a Perkin-Elmer DSC7 calorimeter under continuous-heating conditions using heating rates of 20, 40 and 60 K/min. The calibration procedure for the apparatus ensured that temperature measurements were correct to within <0.05% and the absorbed/released enthalpy was accurate to within ~2%. The reproducibility of the results was higher than 98%. To ensure that the observed irreversible signal was above the detection level of the apparatus, additional third runs were performed on all samples and it was found for each condition that the DSC signals on these third runs were coincident with the second run. Fig. 1 shows typical DSC net signals for ECAP nickel samples using these three different heating rates.

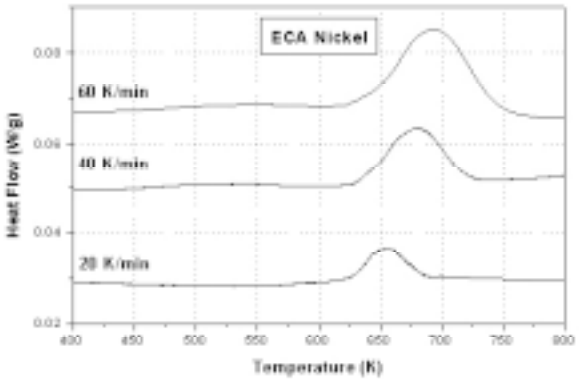

Fig. 1. Typical DSC net signals after subtracting the base line for different heating rates.

3. THEORETICAL CONSIDERATIONS

There are numerous reports documenting the use of DSC in studying the transformations occurring in solids during heating. Two important parameters are usually determined from detailed analyses: (i) the activation energy, E, and (ii) the released (or absorbed) enthalpy, H. The activation energy can be derived from standard Kissinger [9] or Ozawa [10] plots or for isothermal experiments from the Johnson-Mehl-Avrami (JMA) equation [11, 12, 13]. These approaches are different in terms of their physical origins [14] but they lead to similar values for the activation energy. The Kissinger and Ozawa analyses were developed for non-isothermal conditions but they start from the rate equation for the chemical reaction (or reactions of the type: solid $\rightarrow$ solid + gas): $\dot{x} = k(1-x)^n$, where $\dot{x}$ is the rate, x is the fraction reacted, k is a rate constant of the chemical reaction dependent on temperature and n is the empirical order of the reaction. The JMA equation is of the form $x = 1-\exp[-(kt)^n]$ and this generally describes the kinetics of solid-state transformations but it was developed for an analysis of isothermal experiments. In this equation, x is the fraction of the transformation completed at time t, k is a constant associated with the nucleation rate and growth rate, both being dependent on temperature, and n is the power reflecting the nucleation and growth morphology. The integration of the transformation kinetics equation under non-isothermal conditions was developed recently [15]. It is important to note that the most significant error in the calorimetric analysis comes not from the equation selected for the analysis but from the accuracy of the experi-

mental determination of the various parameters within the equation.

This paper presents new results for calculating the apparent activation energy and measuring the released enthalpy in DSC experiments. The apparent activation energy can be derived from the Kissinger plot:

$$d\left(\ln\frac{\beta}{T_P^2}\right)\Big/ d\left(\frac{1}{T}\right) = -\frac{E}{R}, \tag{1}$$

or from the relationship [13]

$$d\left(\ln\frac{\beta}{T_P}\right)\Big/ d\left(\frac{1}{T}\right) = -\frac{E}{R}, \tag{2}$$

where β is the heating rate, T_P is the peak temperature, T is the absolute temperature, E is the apparent activation energy and R is the gas constant. It has been shown [13] that Eq. (2) is more correct for grain growth but the error due to using Eqs. (1) or (2) is less than 3%, which is considerably less than the errors in measurement of the peak temperature, T_P. In the present study Eq. (1) has been employed.

Following Yinnon and Uhlmann [16], the apparent activation energy can be expressed as

$$E \approx \frac{E_N + mE_G}{m+1}, \tag{3}$$

where E_N and E_G are the activation energies for nucleation and grain growth, respectively, and the exponent m is an integer or half-integer depending on the mechanism of grain growth and the dimensionality of the crystal. For interface-controlled grain growth, the value of m is 1. If the nucleation frequency is negligible over the temperature range of the DSC analysis, then $E_N << E_G$ and

$$E_G = 2E. \tag{4}$$

The applicability of Eq. (3) for non-isothermal analysis has been verified [17] when the grain growth rate is controlled by temperature and a system undergoes structurally only a morphological change. This situation is realized during grain growth in pure metals when the chemical composition of moving grain boundaries is not altering.

The enthalpy release is associated with the decrease in the intercrystalline volume fraction due to grain growth and dislocation annihilation processes. Following Wang *et al.* [18], the change in the intercrystalline volume fraction can be expressed in terms of the grain size as

$$\Delta f_{IC} = \left(1-\frac{\delta}{d}\right)^3 - \left(1-\frac{\delta}{d_0}\right)^3, \tag{5}$$

where δ ($\approx 0.8 - 1$ nm) is the grain boundary thickness and d_0 and d are the initial and final grain sizes, respectively. Since $\delta/d << \delta/d_0 << 1$, it follows that Eq. (5) can be rewritten as

$$\Delta f_{IC} = \frac{3\delta}{d_0}. \tag{6}$$

It is possible to deduce the total grain boundary energy released using the following procedure. The grain boundary surface energy, γ, is ~ 0.7 J·m^{-2} [19] and this corresponds to a volume density of $\alpha\gamma/d_0$, where α is a geometrical factor. For an idealized model of spherical grains, $\alpha = 3$ and the grain boundary energy can be represented (in units of J·mol^{-1}) as

$$\Delta H_{GB} = 3\frac{\gamma}{d_0}\Omega N_A, \tag{7}$$

where $\Omega = 1.09\cdot10^{-29}$ m^3 is the atomic volume and N_A is Avogadro's number. For this situation, the elastic energy of the dislocation network, ΔH_{EL}, is the difference between the total measured heat released and the energy associated with the intercrystalline fraction as calculated by Eq. (6). The energy stored in the dislocation network is described by the relationship [20]:

$$E_{EL} = A^* G b \rho \log\frac{R_c}{r_0}, \tag{8}$$

where the coefficient A^* is equal to $1/4\pi$ for screw dislocations and $1/[4\pi(1-\nu)]$ for edge dislocation, G is the shear modulus ($7.89\cdot10^{10}$ Pa), ν is Poisson's ratio, b is the magnitude of the Burgers vector ($2.49\cdot10^{-10}$ m), ρ is the dislocation density, R_C is the effective outer radius for dislocation interactions and $r_0 >> b$ is the dislocation core radius. If the dislocation array is further idealized as a regular square network, as shown in Fig.2, R_C is given by

$$R_C = \frac{1}{2\sqrt{\rho}}, \tag{9}$$

where ρ is now named the "effective" dislocation density. Eq. (9) then becomes

$$E^* = \frac{4E_{EL}}{A^* G} = x\log\left(\frac{1}{\sqrt{x}}\right), \tag{10}$$

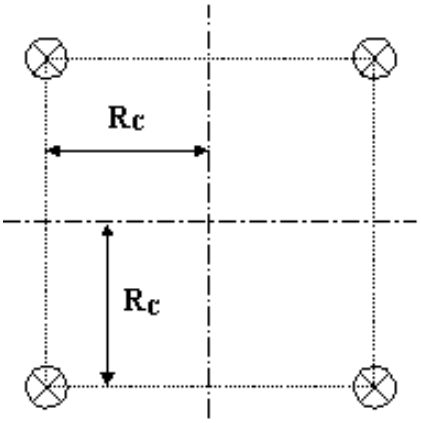

Fig. 2. Idealized scheme of dislocation arrangement in UFG materials.

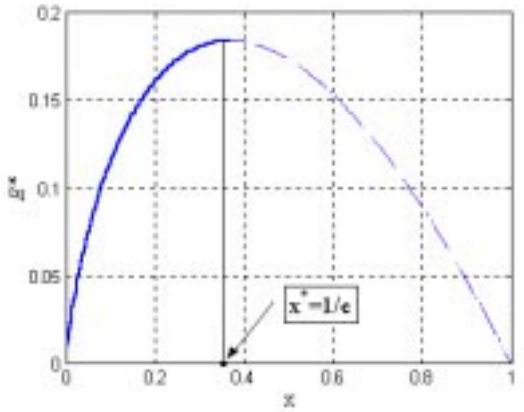

Fig. 3. A plot of normalized elastic energy, E^*, vs. the dimensionless parameter, $x=4b^2\rho$.

where $x = 4b^2\rho$ is a dimensionless parameter. The variation of the term $x\log(1/\sqrt{x})$ with the value of x is shown in Fig. 3 for the interval [0, 1]: it has a maximum at $x^* = 1/e = 0.3679$ and decreases at $x > x^*$. Since a decreasing elastic energy is not physically meaningful, the maximum point corresponds to the maximum possible dislocation density for the material. For nickel, therefore, the maximum dislocation density is estimated as $\rho_{max} = 1/(4b^2e) = 1.5\cdot10^{18}$ m^{-2}. For nickel subjected to processing by severe plastic deformation, the elastic energy of the dislocation array, E_{EL}, is equal to the difference between the measured heat release, ΔH, and the energy stored in the intercrystalline region, ΔH_{GB}. Thus, $E_{EL}=\Delta H - \Delta H_{GB}$, which may be written in the form

$$\frac{4(\Delta H - 3\gamma d_0 \Omega N_A)}{A^* G} = x\log\left(\frac{1}{\sqrt{x}}\right). \qquad (11)$$

Eq. (11) provides an estimate of x and therefore a value for the "effective" dislocation density, ρ.

4. RESULTS AND DISCUSSION

4.1. Transmission electron microscopy

There have been several investigations of the microstructures formed in nickel samples processed by severe plastic deformation including nickel processed by ECAP [3, 4], HPT [2] and electrodeposition [6, 21]. Examination by TEM has revealed several common features associated with these samples. All of these processes lead to highly non-equilibrium microstructures with many grain boundaries that are poorly defined and with grain interiors having complex contrast. These observations suggest a high level of internal stresses and elastic distortions of the crystal lattice. The azimuthal spreading of spots in the selected area electron diffraction (SAED) patterns also indicate the presence of internal stresses whereas the well-defined rings generally present after high imposed strains suggest the grains are primarily separated by boundaries having high angles of misorientation. Materials processed by SPD techniques may also possess distinctive non-homogeneities. Thus, HPT samples generally exhibit some variation in the microstructure between the center and the edge of the disk whereas samples processed by ECAP have an anisotropy of shape along the pressing direction.

In the present investigation, the use of a combination of ECAP and HPT provides an opportunity for removing some of these undesirable properties. For example, Fig. 4 shows a TEM micrograph of nickel after processing through the ECAP + CR + HPT procedure together with an SAED pattern taken from an area having a diameter of 1.8 μm. In this condition, the microstructure is remarkably homogeneous, the mean grain size is ~100 nm and the SAED pattern indicates the presence of high angle boundaries between the grains.

4.1. Differential scanning calorimetry

During continuous heating, the microstructures of the processed materials undergo significant changes in grain size. An example is shown in Fig. 5 for nanocrystalline electrodeposited nickel, where Fig. 5(a) is a bright-field TEM image showing the as-processed grain size of ~35 nm and Fig. 5(b) is an

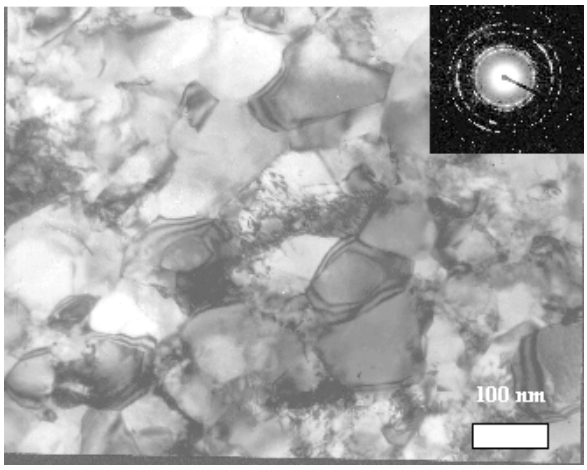

Fig. 4. TEM micrograph of nickel subjected to ECAP (room temperature, 8 passes) + cold rolling (85% reduction in thickness) + HPT (room temperature, 6 GPa, 5 turns).

optical micrograph showing the very large grains, with an average size of ~300 μm, present in this material after three runs from room temperature to 973K at a heating rate of 60 K/min.

Fig. 6 shows the Kissinger plots for all Ni samples studied in this investigation where all of the relevant experimental data are summarized in Table 1. It is apparent from Fig. 6 that the Ni samples subjected to HPT, or to HPT in combination with ECAP or ECAP + CR, exhibit lower temperatures for the grain growth process. By contrast, the ECAP samples exhibit the highest temperatures for grain growth and the electrodeposited samples lie at intermediate positions. A calculation of the activation energy for grain growth through Eqs. (1-4) gives a value for E_G of ~89.2±4.5 kJ/mol for the HPT samples and the other samples prepared by combinations including HPT have even lower values for the activation energy. By contrast, the samples prepared by ECAP and electrodeposition have activation energies close to that for grain boundary self-diffusion in nickel (~115 kJ/mol [22]). The value of the activation energy determined after ECAP nickel is therefore in good agreement with that obtained from isothermal annealing experiments [3]. However, there is a disagreement in the values of the activation energy and the heat release measured in this work and reported earlier by Wang *et al.* [6]. The reason for this discrepancy is not known but it is significant to note that the values measured in this study for the released enthalpy, ΔH, appear to correlate with the initial grain size and thus with the intercrystalline volume fraction. This correlation is demonstrated in Fig. 7 where the released enthalpy,

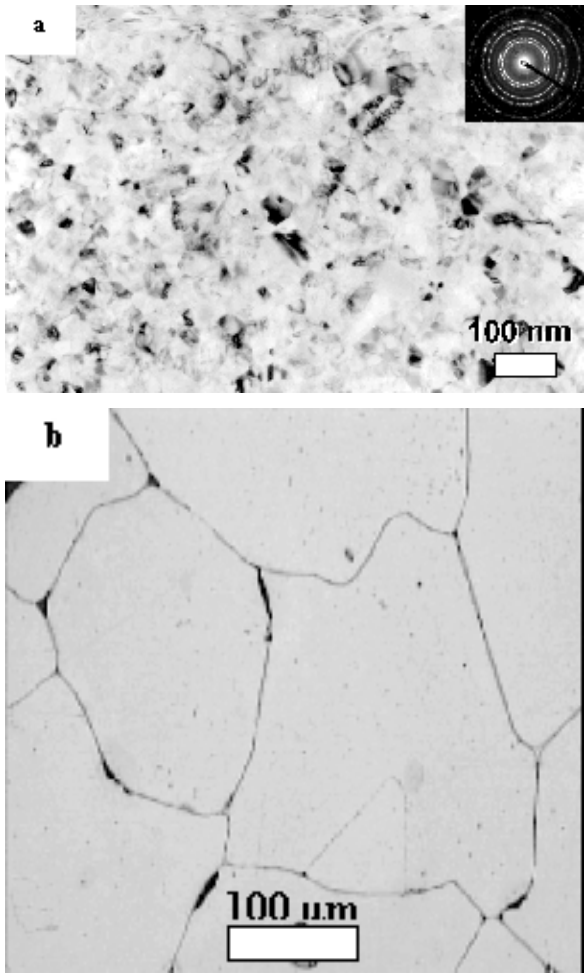

Fig. 5. Electrodeposited nickel: (a) in bright-field TEM before DSC [20] and (b) using optical microscopy after 3 runs at a heating rate of 60 K/min up to the temperature of 923K.

ΔH, and the activation energy, E_G, are plotted as a function of the initial grain size, d_0.

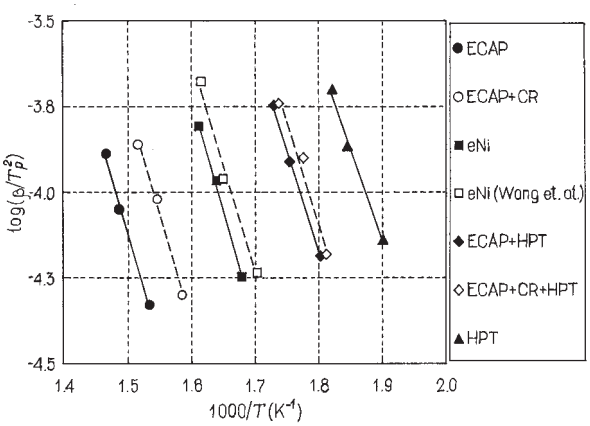

Fig. 6. Kissinger plots for all nickel samples investigated in this study and for electrodeposited nickel (Wang et. al. [6]).

Table 1. Data from DSC studies for materials processed by SPD.

Heating rate β, $K \cdot min^{-1}$	ECAP	ECAP+CR	HPT	ECAP+HPT	ECAP+CR+HPT	eNi	eNi [6]
			Peak temperature T_P, K				
20	652.0	630.4	525.9	554.9	552.0	595.4	587
40	672.9	646.5	542.2	570.3	563.2	609.5	606
60	681.2	659.2	549.0	578.6	575.7	620.7	–
d_0, nm	350 [3]	300	170 [2]	140	100	35 [20]	20 [6]
Δf_{IC}, 10^3	8.6	9.4	17.6	21.4	30.0	85.7	150.0
E_G, $kJ \cdot mol^{-1}$	107.9 ±5.4	105.8 ±5.3	89.2 ±4.5	98.7 ±4.9	97.9 ±4.9	107.8 ±5.4	131.5
ΔH, $J \cdot mol^{-1}$	59.3	75.1	102.7	187.9	229.0	610.6	415.7

It is possible that the mean value of the total enthalpy released is the sum of the grain boundary energy due to the decrease in the intercrystalline volume fraction and the elastic energy of dislocations released due to their annihilation. All of the results calculated from the experimental data using Eqs. (7) to (11) are presented in Table 2. Thus, the effective density of dislocations in these materials after SPD processing is in the range from 10^{13} to 10^{14} m^{-2}. These values are high but nevertheless they are consistent with experimental values reported from x-ray analyses of nanostructured materials [23]. It is important to note that these dislocation densities lead to average separations between neighboring dislocations of ~20 nm in the electrodeposited nickel and ~60 nm and ~80 nm in the nickel processed by HPT and by ECAP, respectively. This distance is therefore comparable with the mean grain size in the electrodeposited nickel so that the interior of a grain may contain only a single dislocation whereas the calculations suggest as many as three and five dislocations within each grain after processing by HPT and by ECAP, respectively. These calculations provide an explanation for the failure to observe dislocations within the interior of grains when there is only complex contrast created by the dislocations.

It is important to highlight two apparent discrepancies in these results. First, from Fig.6 one can infer that HPT nickel has a lower temperature for grain growth compared to the samples denoted as ECAP+HPT and ECAP+CR+HPT. A recent study of grain boundary misorientation distribution [24] showed that in ECAP nickel there is a fraction of low-angle grain boundaries which may be inherited in samples subjected to high-pressure torsion and thus lead to a lower thermal stability. The electrodeposited nickel possesses a smaller grain size (~35 nm) and has a demonstrated higher thermal stability compared to HPT, ECAP+HPT and ECAP+CR+HPT samples. There are two possible explanations for this effect. First, these samples were obtained from the sulfur bath and although the sulfur concentration was below the EDS detectable level it is possible that several dozens ppm of S may be present in solid solution. Moving grain boundaries will lead to a segregation of sulfur impurities creating sulfides and retarding further grain growth. This explanation is reasonable but in fact TEM observations [25] failed to reveal any nickel sulfides in foils prepared from eNi samples heated up to 600K with a heating rate of 40 K/min. The second possible explanation relates to the strong growth texture of (111)

Table 2. Estimates of the dislocation densities in nickel after SPD processing.

Parameters	Grain size, nm					
	35	100	140	170	300	350
ΔH, $J \cdot mol^{-1}$	610.6	229.0	187.9	102.7	75.1	59.3
ΔH_{GB}, $J \cdot mol^{-1}$	265.0	92.7	66.2	54.5	30.9	26.5
E_{EL}, $J \cdot mol^{-1}$	345.6	136.3	121.7	48.1	44.2	32.8
$x=4b^2\rho$, 10^{-4}	6.613	2.607	2.328	0.921	0.845	0.628
ρ, m^{-2}	$6.0 \cdot 10^{14}$	$2.1 \cdot 10^{14}$	$1.9 \cdot 10^{14}$	$6.8 \cdot 10^{13}$	$6.1 \cdot 10^{13}$	$4.0 \cdot 10^{13}$

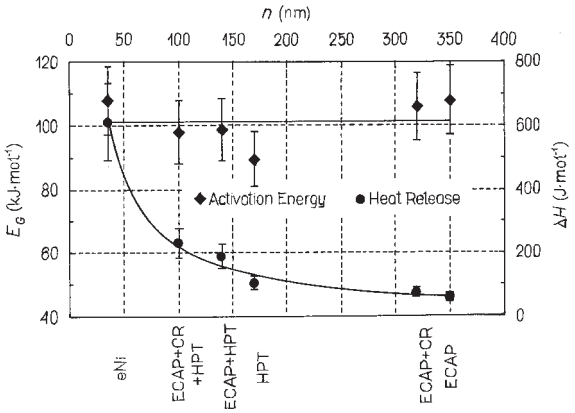

Fig. 7. Values of the activation energy, E_G, and the released enthalpy, ΔH, as a function of the initial grain size, d_0.

that is observed in electrodeposited nickel [26]. It was reported that grain growth in electrodeposited nickel is accompanied by an increase of Σ3 boundaries [26] which may be the origin of the higher thermal stability.

4. CONCLUDING REMARKS

The present investigation leads to a determination of the activation energy for grain growth in ultrafine-grained nickel processed using ECAP, HPT and a combination of these procedures. The temperature associated with the onset of grain growth is generally displaced to lower temperatures as the grain size is reduced. Nickel processed by HPT gives the lowest temperature for the onset of grain growth and thus the lowest activation energy. This appears to be related to the highly non-equilibrium state of the grain boundaries produced by HPT and to the consequent high boundary mobility.

The activation energy associated with grain growth in samples processed by ECAP is close to the value anticipated for grain boundary diffusion in nickel and therefore it is consistent with earlier data. The heat release measured by DSC correlates well with the intercrystalline volume fraction and the stored dislocation density. The values estimated for the effective densities of dislocations in these materials are high, within the range of ~10^{13} to 10^{14} m^{-2} and this is consistent with earlier reports using x-ray measurements.

ACKNOWLEDGEMENTS

This work was supported in part by INTAS under Grant No. 99-1216 and by the U.S. Army Research Ofice under Grant No. DAAD19-00-1-0488. One of the authors (APZ) thanks the DGR of Generalitat of Catalonia for financial support.

REFERENCES

[1] R. Z. Valiev, R. K. Islamgaliev and I. V. Alexandrov // *Prog. Mater. Sci.* **45** (2000) 102.
[2] A. P. Zhilyaev, S. Lee, G. V. Nurislamova, R. Z. Valiev and T. G. Langdon // *Scripta Mater.* **44** (2001) 2753.
[3] A. P. Zhilyaev, G. V. Nurislamova, M. D. Baró, R. Z. Valiev and T. G. Langdon // *Metall. Mater. Trans. A* (2002), in press.
[4] K. Neishi, Z. Horita and T. G. Langdon // *Mater. Sci. Eng. A* **325** (2002) 54.
[5] Yu. R. Kolobov, G. P. Grabovetskaya, M. B. Ivanov, A. P. Zhilyaev and R. Z. Valiev // *Scripta Mater.* **44** (2001) 873.
[6] N. Wang, Z. Wang, K. T. Aust and U. Erb // *Acta Mater.* **45** (1997) 1655.
[7] M. C. Iordache, S. H. Whang, Z. Jiao and Z. M. Wang // *Nanostructured. Mater.* **11** (1999) 1343.
[8] Y. Iwahashi, Z. Horita, M. Nemoto and T. G. Langdon // *Acta Mater.* **46** (1998) 3317.
[9] H. E. Kissinger // *Anal. Chem.* **29** (1957) 1702.
[10] T. J. Ozawa // *Thermal. Anal.* **2** (1970) 301.
[11] W. A. Johnson and K. F. Mehl // *Trans. AIME.* **135** (1939) 416.
[12] M. J. Avrami // *J. Chem. Phys.* **7** (1939) 1102. *Ibid.* **8** (1940) 212. *Ibid.* **9** (1941) 177.
[13] L. C. Chen and F. Spaepen // *J. Appl. Phys.* **69** (1991) 679.
[14] J. A. Augis and J. E. Bennet // *J. Thermal. Anal.* **13** (1978) 283.
[15] J. Vázquez, C. Wagner, P. Villares and R. Jiménez-Garay // *Acta mater.* **44** (1996) 4807.
[16] H. Yinnon and D. R. Uhlmann // *J. Non-Cryst. Solids.* **54** (1983) 253.
[17] D. W. Henderson // *J. Non-Cryst. Solids.* **30** (1979) 301.
[18] N. Wang, G. Palumbo and Z. Wang // *Scripta Metal. Mater.* **28** (1993) 253.
[19] M. W. Grabski and R. Korski // *Phil. Mag.* **22** (1975) 707.
[20] J.P. Hirth and J. Lothe, *Theory of Dislocations* (McGraw-Hill, New York, 1968).
[21] S. X. McFadden, A. P. Zhilyaev, R. Mishra and A. K. Mukherjee // *Mater. Lett.* **45** (2000) 345.
[22] A. R. Wazzan // *J. Appl. Phys.* **36** (1965) 3596.

[23] Kh. Ya. Mulykov, G. F. Korznikova, R. Z. Abdulov and R. Z. Valiev // *J. Magnetism Magnet. Mater.* **89** (1990) 207.
[24] A. P. Zhilyaev, B.-K. Kim, G. V. Nurislamova, M. D. Baro, J. A. Szpunar and T. G. Langdon // *Scripta Mater.* **46** (2002) 575.
[25] S.X. McFadden, private communication.
[26] B.-K. Kim and J. A. Szpunar // *Proc. of the First Joint Intern. Conf. On Recrystallization and Grain Growth (ReX & GG)*, Aachen, Germany (2001) – in press.